


Dielectric relaxation effect on flow behavior of electrorheological fluids

Zhiyuan Wang¹, Xinglong Gong¹, Fan Yang¹,
Wanquan Jiang² and Shouhu Xuan¹

Journal of Intelligent Material Systems and Structures
2015, Vol. 26(10) 1141–1149
© The Author(s) 2014
Reprints and permissions:
sagepub.co.uk/journalsPermissions.nav
DOI: 10.1177/1045389X14536007
jim.sagepub.com


Abstract

The dielectric relaxation effect on the flow behavior of electrorheological fluids under dynamic shear was studied. The flow curves of electrorheological fluids in the dynamic state were simulated with shear rates from 0.1 to 1000 s⁻¹ under different relaxation times. When the magnitude of the relaxation time is smaller than 10⁻² s, the break shear rate changes little at different relaxation times. But the break shear rate changes obviously when the magnitude of the relaxation time is larger than 10⁻² s. To further understand the influence of the relaxation time, Sr/Ba-doped TiO₂ electrorheological fluids were prepared and their dielectric properties and flow curves under shear flow were tested. The relaxation time of the electrorheological fluid is influenced by the Sr/Ti mole ratio but not the Ba/Ti mole ratio, and the electrorheological effects of the fluids were highly influenced by varying the Sr/Ti mole ratios. The experimental results agreed well with the above computer simulation. Finally, a possible mechanism was proposed to explain the effect of dielectric relaxation on flow behavior of electrorheological fluids.

Keywords

Electrorheological fluids, break shear rate, relaxation time, flow curve

Introduction

Electrorheological fluids (ERFs), typically smart materials, are composed of microsized or nanosized dielectric particles dispersed in a liquid with a low dielectric constant (Halsey, 1992; Jiang et al., 2009, 2011; Wen et al., 2003). When an electric field is applied, the randomly dispersed particles are rearranged along the field direction and form complex column-like structures, which dramatically changes the apparent viscosity. The change is fast (milliseconds) and reversible, which makes the ERFs desirable for technological and industrial applications (Melrose, 1991; Tao and Sun, 1991; Weiss et al., 1993). During the past decades, various inorganic particles, liquid crystals, and polymers were used for preparation of ERFs (Choi and Jhon, 2009), and they were widely applied in damping devices (dampers of engine mounts); force transfers such as clutches, valves, and brakes; and other hydraulic systems or micro-robotics (Choi et al., 1990; Papadopoulos, 1998).

ER effect results from the formation of particles' chain structure during the application of electric field. Several theoretical models, such as electric double-layer model (Klass and Martinek, 1967), water bridge model (Stangroom, 1983), and polarization model (Davis, 1992; Parthasarathy and Klingenberg, 1996) have been

developed to explain the formation mechanism of chain structure. Among them, the polarization model was believed to be one of the most acceptable models, in which the ER effect was controlled by dielectric mismatch. The higher the dielectric mismatch, the stronger the ER effect is. Therefore, the dielectric properties of suspensions dominate the ER effect. Many research studies were concentrated on how the particles' dielectric properties influence the ER effect. By comparing different kinds of ERFs, Ikazaki et al. (1998) pointed out that the relaxation frequency was in the range from 10² to 10⁵ Hz when the ERF had a large ER effect, and this effect increased with increasing difference between the dielectric constants below and above the relaxation frequency. Hao and colleagues (Hao, 1997; Hao et al.,

¹CAS Key Laboratory of Mechanical Behavior and Design of Materials, Department of Modern Mechanics, University of Science and Technology of China (USTC), Hefei, China

²Department of Chemistry, University of Science and Technology of China (USTC), Hefei, China

Corresponding author:

Xinglong Gong, CAS Key Laboratory of Mechanical Behavior and Design of Materials, Department of Modern Mechanics, University of Science and Technology of China (USTC), Hefei 230027, China.
Email: gongxl@ustc.edu.cn

1999; Hao and Xu, 1996) developed a dielectric loss model to study the dielectric relaxation influence on the ER effect and found that the ERF with a larger dielectric loss constant exhibited a larger ER effect. Cho et al. (2003) prepared the monodisperse polymer microspheres (PAPMMAs)-based ERFs and studied the dielectric relaxation time, polarizability, and Cole-Cole plot from the dielectric spectra. All the analysis indicated that there must be an inherent and natural connection between the dielectric relaxation of the ERF and its ER effect. However, the detailed mechanism of the dielectric relaxation effect on the ERFs is still unclear.

Moreover, the experiment can directly prove the connection between the particles' characteristics and their ER properties. A large amount of research has been done to change the ER effects by modifying the ER particles. Wang et al. (2013) investigated the dielectric behaviors of TiO₂ ERFs with different TiO₂ polymorphs and found that rutile should have better ER activity than anatase by analyzing dielectric spectroscopy. Di et al. (2006) prepared a urea-doped mesoporous TiO₂ ERF showing a high ER behavior under an applied electric field. The dielectric spectra analysis showed this suspension had a large difference in the dielectric constant below and above the relaxation frequency, and the maximum value of the dielectric loss tangent of the particle was larger than 0.1. Yin and Zhao (2006) prepared a new mesoporous Cr-doped TiO₂ ER material and its ER efficiency was far superior to that of the nonporous pure TiO₂ ER suspension because it possessed a significantly larger interfacial polarizability. It was found that the dielectric property of the dispersed particles was tunable by varying the doped metal ions, thus ERFs with different dielectric property could be prepared by particle modification, which is also favored for investigating the mechanism of the dielectric relaxation effect on the ERFs.

In this article, a computer simulation and an experiment were both conducted to study the dielectric relaxation effect on flow behavior of ERFs. The computer simulation showed that the break shear rate of ERFs decreased drastically when the magnitude of relaxation time exceeded 10⁻² s. However, when the relaxation time is smaller than 10⁻² s, this influence could be neglected. The Sr/Ba-doped ERFs were further prepared to investigate the dielectric relaxation effect and the experimental results matched the simulated shear curves quite well. Finally, a possible mechanism was proposed and the dielectric relaxation effect on the ERFs was discussed.

Experiment

The ERFs used in this experiment were made of Sr/Ba-doped TiO₂ particles in silicone oil with the volume

fraction of 20%. Various moles of SrNO₃/BaCO₃ were added during preparation of TiO₂ particles to obtain needed Sr/Ba-doped TiO₂ particles. The viscosity and the dielectric constant of silicone oil are 0.1 Pa S and 2.6, respectively. The rheological behavior of the suspension was investigated by a rotational rheometer (Physica MCR 301; Anton Paar), ER HVS/ERD 180, and the CC10-E accessory. The dielectric data were measured by ModuLab-MTS (Advanced Measurement Technology, Inc.).

Model

A model ER system studied in this article is supposed to consist of N interacting spherical particles of dielectric constant ϵ_p and diameter σ , suspended in a silicone oil fluid of dielectric constant ϵ_f ($\epsilon_f < \epsilon_p$) and viscosity η_f . The model system is in a box with its volume $V = L_x \times L_y \times L_z$, confined between the two parallel electrodes at $z = 0$ and L_z . An external electric field is applied along the z -direction. A steady shear rate $\dot{\gamma}$ is also imposed along the x -direction (parallel with the plate). Here, the velocity field is varied linearly along the z -direction (the top electrode moves at a speed of $\dot{\gamma}L_z$). Because the particles are much larger than the liquid molecule, it is thought that slip happens between the particles and the electrodes but not between the liquid molecules and the electrodes. Before the application of the electric field, particles are randomly dispersed in the medium fluid.

The motion of i th particle having mass m at time t and position $\mathbf{r}_i(t)$ is described by the following classical equation of motion (Guo et al., 1996)

$$\frac{m d^2 \mathbf{r}_i}{dt^2} = \mathbf{F}_i - 3\pi\sigma\eta_f \left(\frac{d\mathbf{r}_i}{dt} - \dot{\gamma} z_i \hat{x} \right) + \mathbf{R}_i \quad (1)$$

where \mathbf{F}_i is the total force acting on the i th particle, the second term is the Stokes drag, and the last term is the Brownian random force. The Brownian force \mathbf{R}_i is determined independently by a normal distribution with $\langle R_{i,\alpha}(0) \rangle = 0$ and $\langle R_{i,\alpha}(0) R_{i,\beta}(t) \rangle = 6\pi k_B T \sigma \eta_f \delta_{\alpha\beta} \delta(t)$, where $\langle \dots \rangle$ denotes an ensemble average, k_B is the Boltzmann constant, and T is the absolute temperature. Under the electric field E_0 applied along the z -direction, each particle gets an induced dipole moment $\mathbf{p} = (1/2)\pi\beta\epsilon_0\epsilon_f\sigma^3\mathbf{E}_{loc}$ in the fluid with relative dielectric constant ϵ_f where $\beta = (\epsilon_p - \epsilon_f)/(\epsilon_p + 2\epsilon_f)$ and \mathbf{E}_{loc} is the local field, with $\mathbf{E}_{loc} = E_0\hat{z}$ if $\beta \ll 1$.

In a shear flow of shear rate $\dot{\gamma}$, a spherical sphere spins at an angular velocity of $\omega = \dot{\gamma}/2(\boldsymbol{\omega} = \omega\hat{y})$ (Dassanayake et al., 2004). Because the rotational motion that leads to a displacement of its polarized charges on the surface and the relaxation of the surface charges, the rate of change in the dipole moment of the rotating dielectric sphere in an electric field is given by (Wan et al., 2000)

$$\frac{d\mathbf{p}}{dt} = \boldsymbol{\omega} \times \mathbf{p} - \frac{(\mathbf{p} - \mathbf{p}_0)}{\tau} \quad (2)$$

where the dipole moment $\mathbf{p} = p_x \hat{x} + p_z \hat{z}$ at the steady state is expressed as

$$p_x = \frac{\omega \tau p_0}{1 + (\omega \tau)^2}, p_z = \frac{p_0}{1 + (\omega \tau)^2} \quad (3)$$

where τ is the relaxation time. In the rotational state, there is a tilt angle φ between the dipole moment and

The dipolar force acting on the i th particle from the image particle at \mathbf{r}_j is given by

$$\mathbf{F}_{ij}^{el,im} = F_0 \left(\frac{\sigma}{r_{ij}} \right)^4 \{ [\cos 2\varphi - 3 \cos(\theta_{ij} - \varphi) \cos(\theta_{ij} + \varphi)] \hat{r} - \sin 2\theta_{ij} \hat{\theta} \} \quad (9)$$

Now, the total force \mathbf{F}_i in equation (1) is given by

$$\begin{cases} \mathbf{F}_i = \sum_{j(j \neq i)} (\mathbf{F}_{ij}^{el} + \mathbf{F}_{ij}^{rep}) + \sum_j \mathbf{F}_{ij}^{el,im} + \mathbf{F}_i^{wall} + \mathbf{F}_i^{fric}, & \text{for boundary particles} \\ \mathbf{F}_i = \sum_{j(j \neq i)} (\mathbf{F}_{ij}^{el} + \mathbf{F}_{ij}^{rep}) + \sum_j \mathbf{F}_{ij}^{el,im} + \mathbf{F}_i^{wall}, & \text{for the others} \end{cases} \quad (10)$$

the z -direction with $tg\varphi = \omega\tau$. For the rotational particles, the dipolar force acting on the i th particle due to the j th particle at \mathbf{r}_j is given by

$$\mathbf{F}_{ij}^{el} = F_0 \left(\frac{\sigma}{r_{ij}} \right)^4 \{ [1 - 3 \cos^2(\theta_{ij} - \varphi)] \hat{r} - \sin[2(\theta_{ij} - \varphi)] \hat{\theta} \} \quad (4)$$

where $p = |\mathbf{p}|$, $\mathbf{r}_{ij} = \mathbf{r}_i - \mathbf{r}_j$, and $r_{ij} = |\mathbf{r}_{ij}|$; θ_{ij} is the angle between \mathbf{r}_{ij} and z -axis; $\hat{r} = \mathbf{r}_{ij}/r_{ij}$; and $F_0 = 3p^2/(4\pi\epsilon_0\epsilon_f\sigma^4)$.

To simulate the hard spheres and the hard sphere–hard wall interactions, an exponential short-range repulsive force between particles i and j is introduced as (Guo et al., 1996)

$$\mathbf{F}_{ij}^{rep} = 2F_0 \left(\frac{\sigma}{r_{ij}} \right)^4 \exp\left[-100\left(\frac{r_{ij}}{\sigma - 1}\right)\right] \hat{r} \quad (5)$$

and between particle i and the two electrodes

$$\begin{aligned} \mathbf{F}_i^{wall} &= 2F_0 \left(\frac{\sigma}{z_i} \right)^4 \exp\left[-100\left(\frac{r_{ij}}{\sigma - 0.5}\right)\right] \hat{z} \\ &- 2F_0 \left[\frac{\sigma}{L_z - z_i} \right]^4 \exp\left\{-100\left[\frac{L_z - z_i}{\sigma - 0.5}\right]\right\} \hat{z} \end{aligned} \quad (6)$$

For the boundary particles, the friction force between the boundary particles and the electrodes is expressed as (Gong et al., 2011)

$$\begin{cases} \mathbf{F}_i^{fric} = \mu \mathbf{N}_i, & \text{when } N_i > 0 \\ \mathbf{F}_i^{fric} = 0, & \text{when } N_i \leq 0 \end{cases} \quad (7)$$

N_i is the normal force acting on the i th boundary particle

$$\begin{cases} N_i = \sum_{j(j \neq i)} (\mathbf{F}_{ij}^{el} + \mathbf{F}_{ij}^{rep}) \cdot \hat{z}, & \text{for Cathode} \\ N_i = - \sum_{j(j \neq i)} (\mathbf{F}_{ij}^{el} + \mathbf{F}_{ij}^{rep}) \cdot \hat{z}, & \text{for Anode} \end{cases} \quad (8)$$

To study the parametric properties of many different ERFs, we define dimensionless quantities to scale equation (1): $\mathbf{r}_i^* = \mathbf{r}_i/\sigma$, $t^* = t/[3\pi\eta_f\sigma^3/(k_B T)]$, $\mathbf{R}_i^* = \mathbf{R}_i/(k_B T/\sigma)$, and $\mathbf{F}_i^* = \mathbf{F}_i/[p^2/(\epsilon_0\epsilon_f\sigma^4)]$. So, equation (1) can be rewritten as

$$\frac{Ad^2\mathbf{r}_i^*}{dt^{*2}} = Q\mathbf{F}_i^* - \frac{d\mathbf{r}_i^*}{dt^*} + 8\text{Pez}_i^*\hat{x} + \mathbf{R}_i^* \quad (11)$$

where $A = mk_B T/(3\pi\eta_f\sigma^2)^2$, $Q = p^2/(\epsilon_0\epsilon_f\sigma^3 k_B T)$, and $\text{Pe} = 3\pi\eta_f\sigma^3\dot{\gamma}/(8k_B T)$. For most real parameters of ERFs, the magnitude of A in equation (11) is very small ($\sim 10^{-10}$), so in the following simulations we neglect this inertial effect. Thus, it is simplified as

$$\frac{d\mathbf{r}_i^*}{dt^*} = Q\mathbf{F}_i^* + 8\text{Pez}_i^*\hat{x} + \mathbf{R}_i^* \quad (12)$$

Equation (12) is integrated with a time step $\Delta t^* \leq 0.01/(F_{\max}^* Q)$ using Euler's method; F_{\max}^* is the dimensionless maximum interparticle force that acts on particles, thus the maximum displacement of particles cannot exceed 0.01σ . Periodic boundary conditions are imposed in the x - and y -directions, reflecting boundary conditions in the z -direction.

In the dynamic state, rheological properties are determined by the effective viscosity $\eta_{eff} = \langle \tau_{zx}/\dot{\gamma} \rangle$, where τ_{zx} is the component of the stress tensor, which is an averaged value of the simulations. By using the Bingham model, τ_{zx} is expressed as $\tau_{zx} = \tau_E + \eta_s \dot{\gamma}$, where η_s is the viscosity of suspensions (without an electric field). But for these flow curves performed later, the Bingham fluid model is not able to fit them well. Therefore, Cho–Choi–Jhon (CCJ) model will be better (Cho et al., 2005). In order to definitely understand the relationship of the particle interactions, we focused on the electric field–induced shear stress τ_E , which was calculated by equation (13) (Sun et al., 2006)

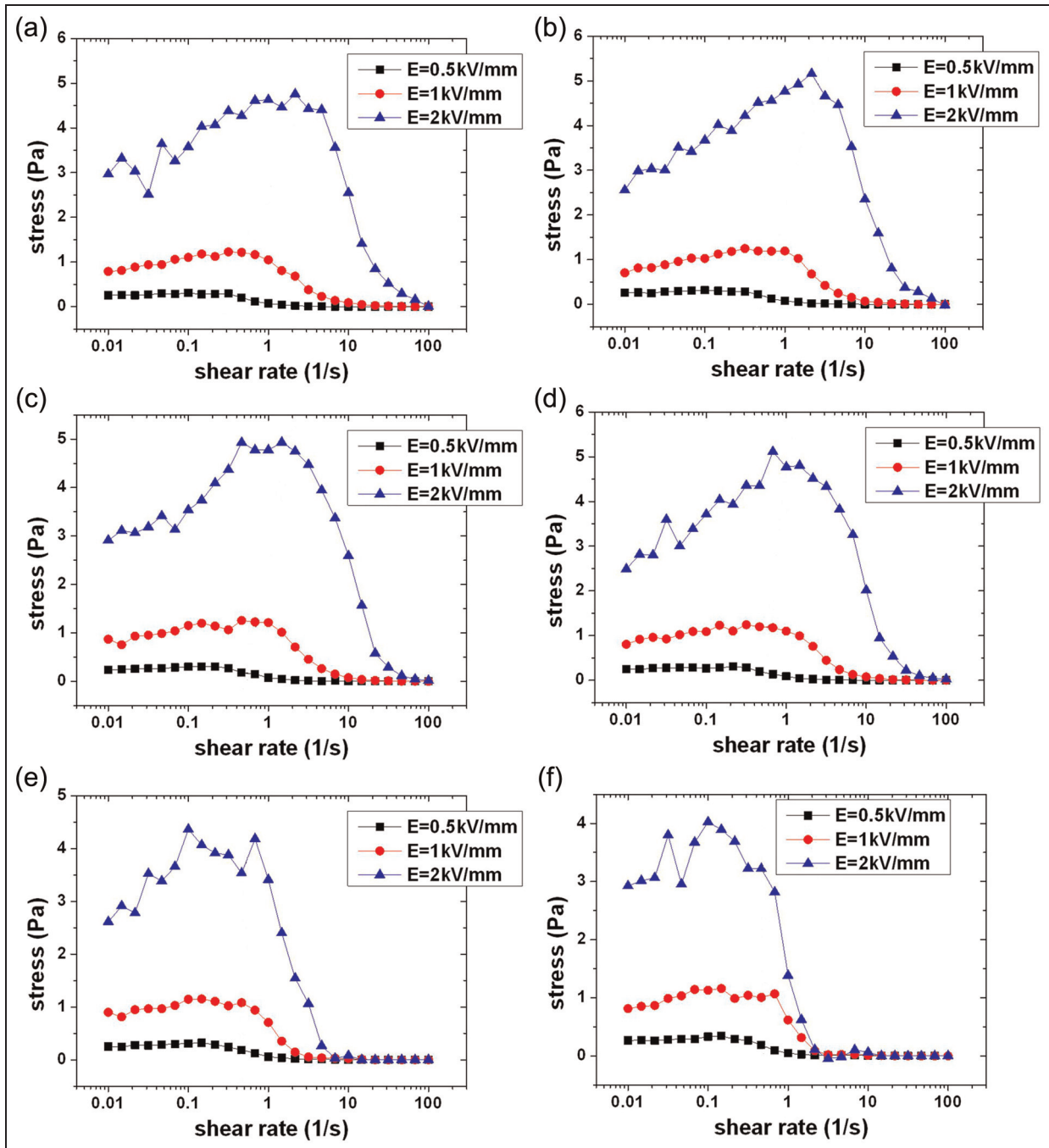


Figure 1. Simulation results of shear stress versus shear rate at different relaxation times: (a) 2×10^{-7} s, (b) 2×10^{-4} s, (c) 2×10^{-3} s, (d) 2×10^{-2} s, (e) 0.2 s, and (f) 0.4 s.

$$\tau_E = \left\langle -\frac{1}{V} \sum_{i=1}^N (\mathbf{r}_i)_z (\mathbf{F}_i^{el})_x \right\rangle \quad (13)$$

Results and discussion

Our simulations have been done for the parameters: $T = 300$ K, $\varepsilon_p = 100$, $\varepsilon_f = 2$, $\sigma = 1 \mu\text{m}$, $\eta_f = 0.1$ Pa s, and $\mu = 0.4$ and carried out in a three-dimensional box ($L_x = 15\sigma$, $L_y = 5\sigma$, $L_z = 15\sigma$) with a system of

$N = 240$ particles (20 stick to the top electrode and 20 stick to the bottom electrode).

Figure 1 shows the relation between the shear stress and the shear rate under different relaxation times and electric field strength through simulation. When the relaxation time is small, these flow curves show a trembling shear behavior, in which the shear stress increases and decreases with shear rate (Ko et al., 2008). Here, the shear stress decreases above a certain shear rate. This shear rate, which is defined as the break shear rate,

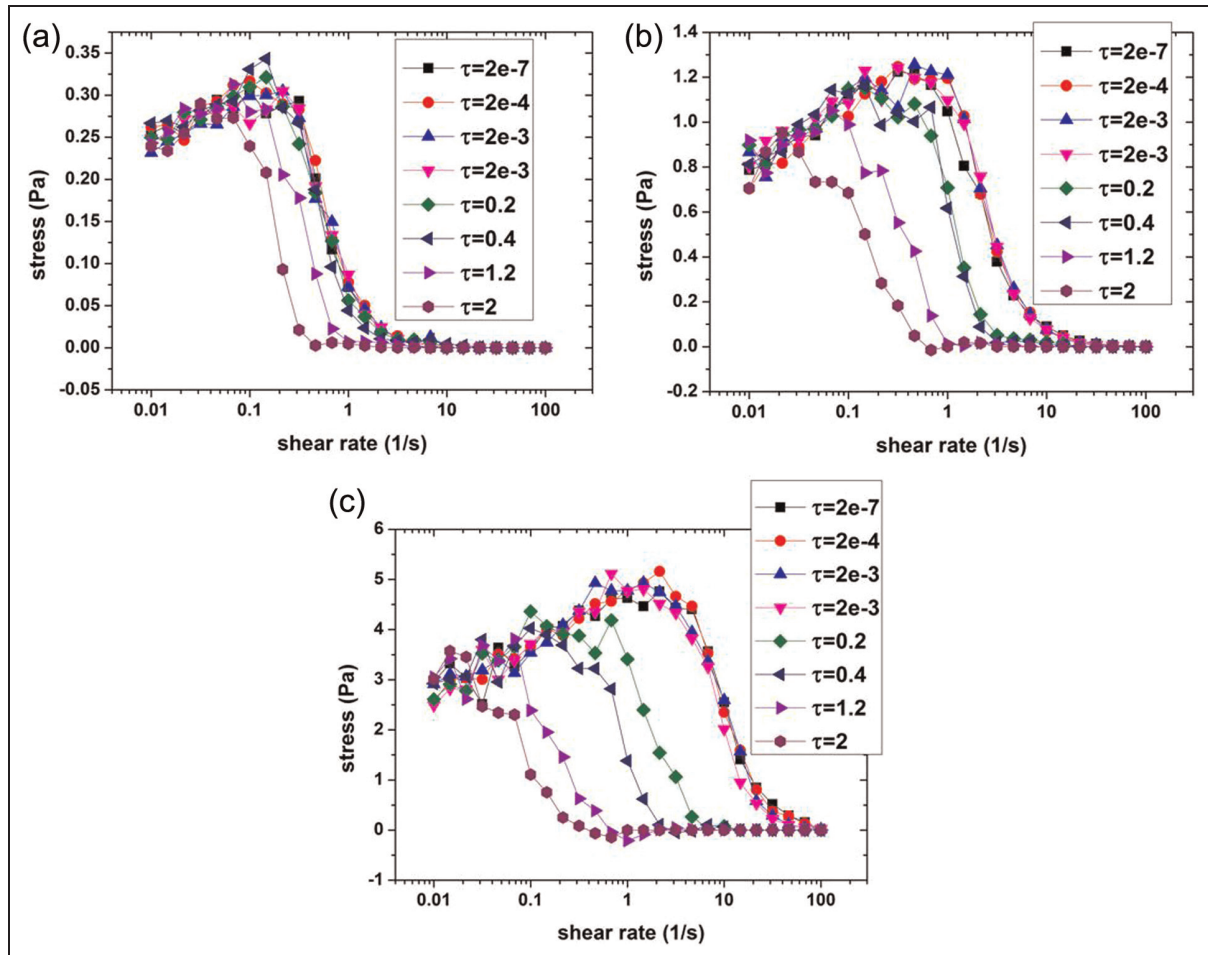


Figure 2. Relaxation time effect on shear stress–shear rate relationship at different electric fields: (a) $E = 0.5$ kV/mm, (b) $E = 1$ kV/mm, and (c) $E = 2$ kV/mm.

is proportional to the square of the electric field in quasi-static state, according to our previous research (Yang et al., 2011). Then, with the increase in the relaxation time, the break shear rate decreases gradually. This means that the ability of resisting breakage of the chains is weakened because of the increase in relaxation time. When the magnitude of the relaxation time exceeds 10^{-2} s, the break shear rate depends on the relaxation time, instead of the electric field. Therefore, the break shear rate of the chains depends on electric and relaxation time together when the magnitude of the relaxation time is less than 10^{-2} s, and the break shear rate is only decided by the relaxation time when it is greater than 10^{-2} s.

Figure 2 is the transformed data of Figure 1, which shows the relaxation time effect on the break shear rate at different electric fields. We find the change occurs between 0.002 and 0.2 s. When the dielectric relaxation time is smaller than 0.002 s, the curves overlap together; then, the curves are distributed dispersedly when the dielectric relaxation time is larger than 0.2 s. Thus, we deduce that the critical state of the dielectric relaxation

time is the magnitude of 10^{-2} s. When the magnitude of the relaxation time is less than 10^{-2} s, the break shear rate changes little at different relaxation times. The break shear rate changes obviously when the magnitude of the relaxation time is greater than 10^{-2} s. With the increase in the relaxation time, the break shear rate decreases and the shear stress decreases at the same time, indicating that the structure strength of the chains is decreasing. Therefore, the ER effect is weakened because of the increase in the relaxation time. It was reported that the relaxation frequency is in the range from 10^2 to 10^5 Hz whenever the ERF has an obvious ER effect, and this effect increases with increased difference between the dielectric constants below and above the relaxation frequency (Ikazaki et al., 1998), which agreed well with our results. In comparison to large electric field, the relaxation time effect on the break shear rate at a small electric field is less obvious because the chains of ERFs are not completely formed at a small electric field. Therefore, Figure 2(a) only shows the changes in the incomplete chain structure of ERFs.

The decrease in the break shear rate means that the structure of the ERF is broken at a smaller shear rate. The nonlinear rheological behavior of the ERF after

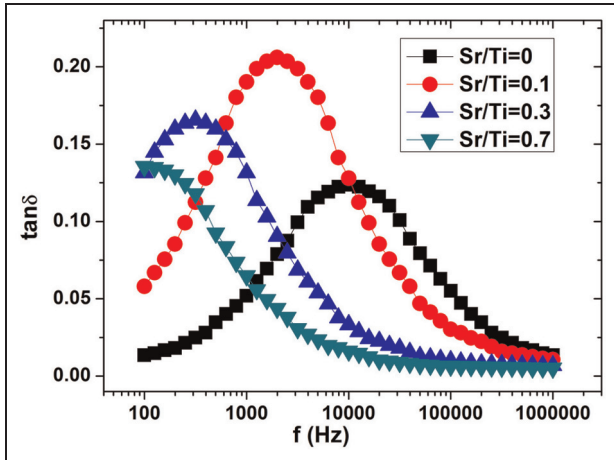


Figure 3. Curves of dielectric loss angle and response frequency of Sr-doped TiO₂ ER materials synthesized with different Sr/Ti mole ratios. ER: electrorheological.

shear yield is caused by the special chain structure. As soon as the break shear rate is achieved, the chains are broken, then the shear stress reduces fast and the ERF becomes a Newtonian fluid from a non-Newtonian fluid. So, a larger relaxation time leads to a smaller break shear rate, and then the ERF works in a smaller efficient range.

Figure 3 shows the relation of the dielectric loss angle and the response frequency of Sr-doped TiO₂-based ER materials with different Sr/Ti mole ratios. The $\tan \delta$ peak is related to the proper polarization response denoted by the relaxation time $\tau = 1/2\pi f_{\max}$, where f_{\max} is the local frequency of the $\tan \delta$ peak (Wu et al., 2012). Therefore, the response frequency is inversely proportional to the relaxation time. The response frequency decreases with the increase in the Sr/Ti mole ratio. When the mole ratio reaches 0.7, the response frequency is smaller than 100 Hz; so, the order of relaxation time is less than 10^{-2} s. Figure 4 presents the flow curves of 20 v/v% Sr-doped TiO₂ ERF with different Sr/Ti mole ratios. When the Sr/Ti mole ratio is 0 or 0.1 (Figure 4(a) and (b)), the ERF shows a trembling shear behavior, in which the break shear rate is

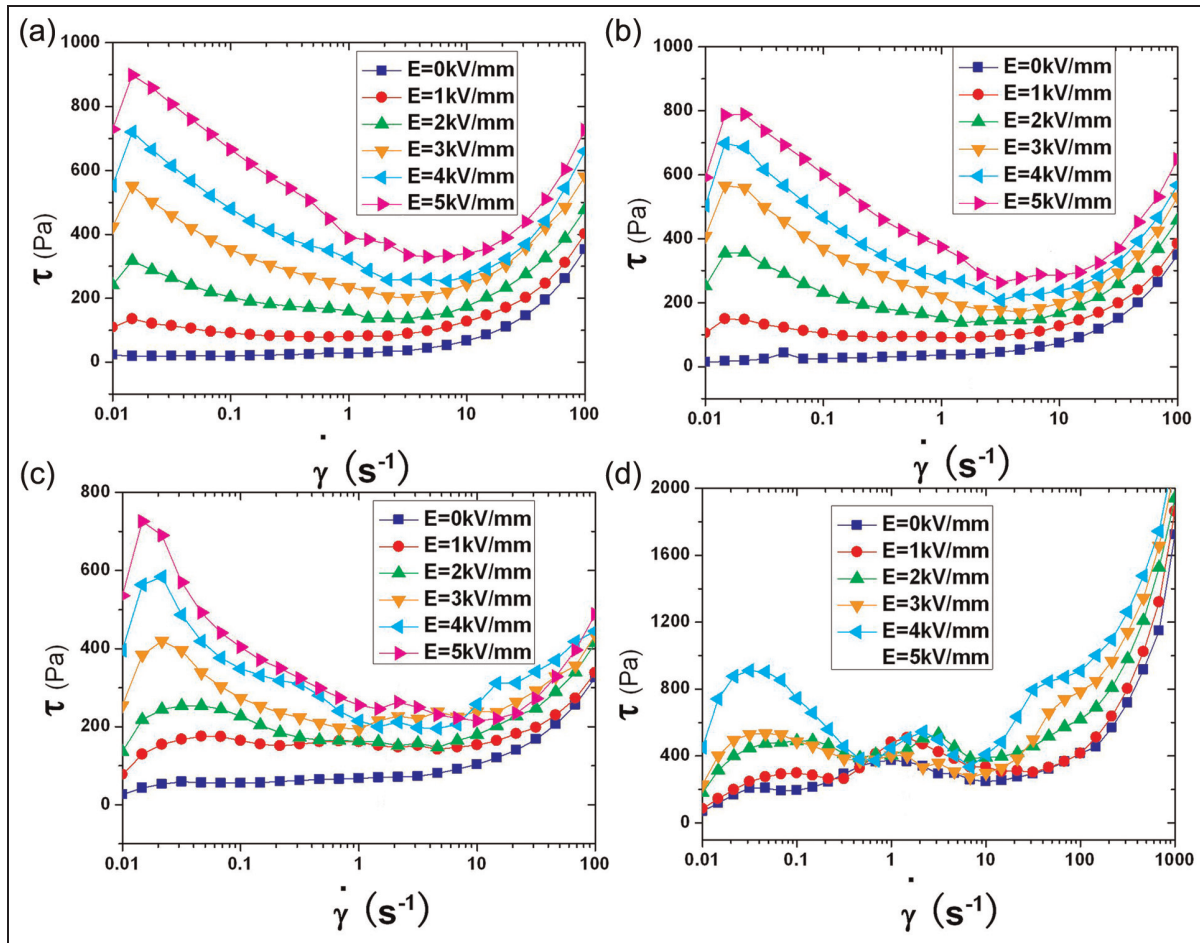


Figure 4. Flow curves of Sr-doped TiO₂ ERF with different Sr/Ti mole ratios: (a) Sr/Ti = 0, (b) Sr/Ti = 0.1, (c) Sr/Ti = 0.3, and (d) Sr/Ti = 0.7.

proportional to the square of the electric field. When the Sr/Ti mole ratio is 0.7 (Figure 4(d)), the break shear rate is almost not influenced by the electric field.

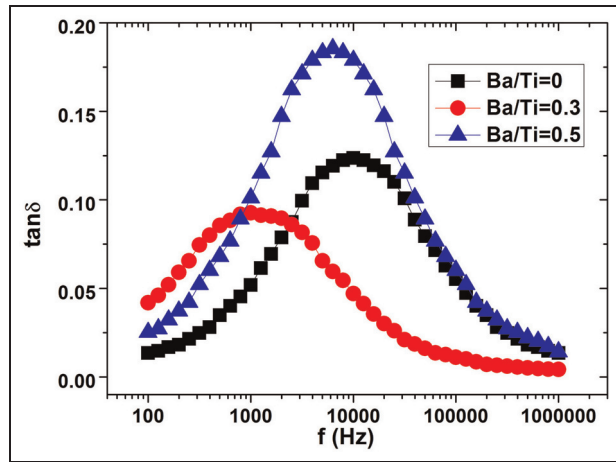


Figure 5. Curves of dielectric loss angle and response frequency of Ba-doped TiO₂ ER materials synthesized with different Ba/Ti mole ratios.

Figure 4(c) can be seen as a transitional state. The change in the curves of the ERF is decided by the relaxation time. The break shear rate depends on electric and relaxation time together when the magnitude of the relaxation time is less than 10⁻² s, then the break shear rate is only decided by the relaxation time when the time is greater than 10⁻² s. Clearly, this experimental research matches our simulation results very well.

Figures 5 and 6 are experiment results of Ba-doped TiO₂ ERF. In Figure 5, the response frequency is in the range from 10² to 10⁵ Hz and almost not influenced by the Ba/Ti mole ratio. This means the Ba/Ti mole ratio cannot change the relaxation time of this ERF. In Figure 6, all the flow curves show a trembling shear behavior and present similar properties with the Ba/Ti mole ratios of 0, 0.3, or 0.5. Therefore, the ERFs with same relaxation time have similar property. This result further suggests that the dielectric relaxation affects the flow behavior of the ERF.

The mechanism of dielectric relaxation effect on the flow behavior of ERFs is further studied in this work (Figure 7). When the electric field exists alone, the chain structure is formed and the electric dipole moment is

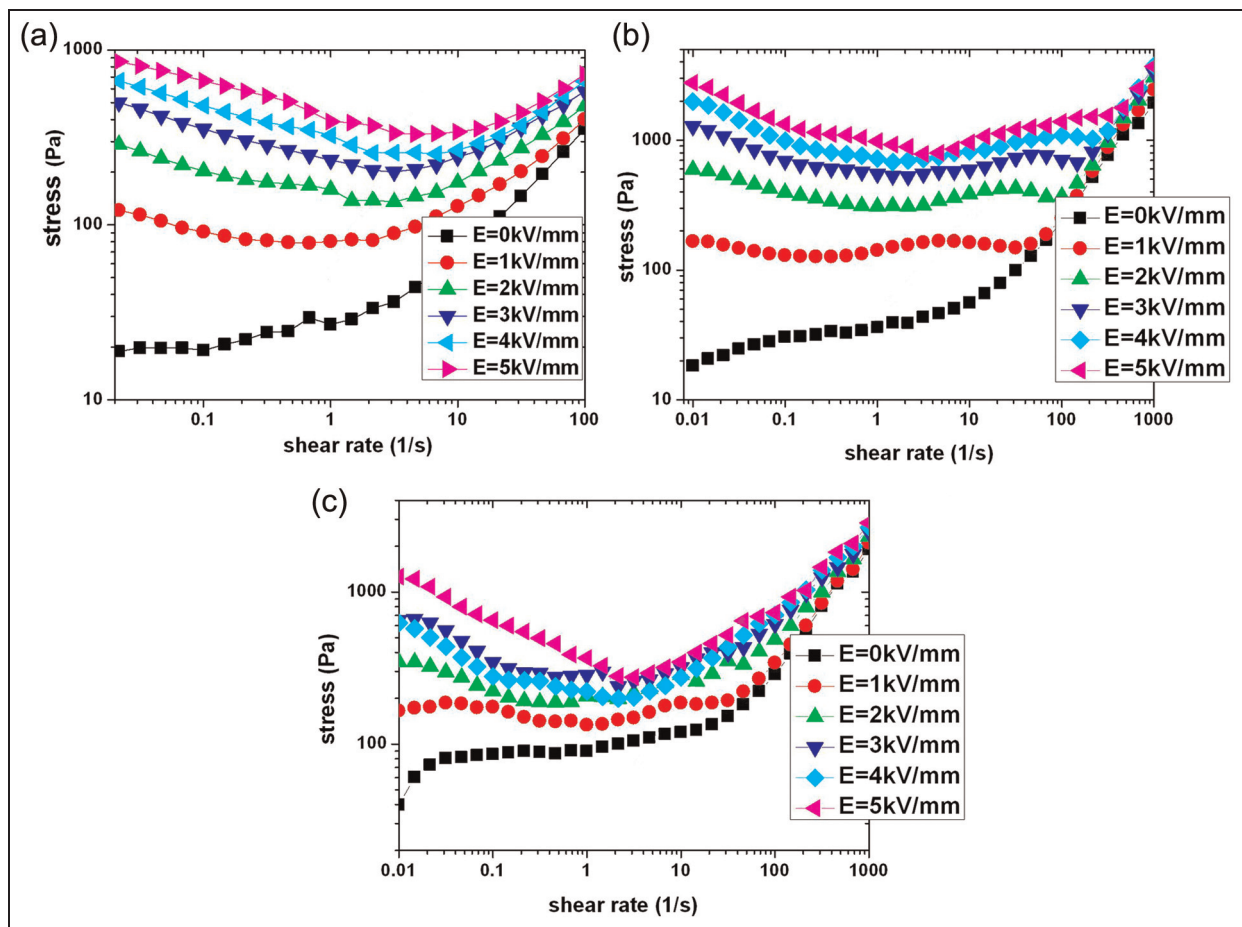


Figure 6. Flow curves of Ba-doped TiO₂ ER fluid with different Ba/Ti mole ratios: (a) Ba/Ti = 0, (b) Ba/Ti = 0.1, and (c) Ba/Ti = 0.3. ER: electrorheological.

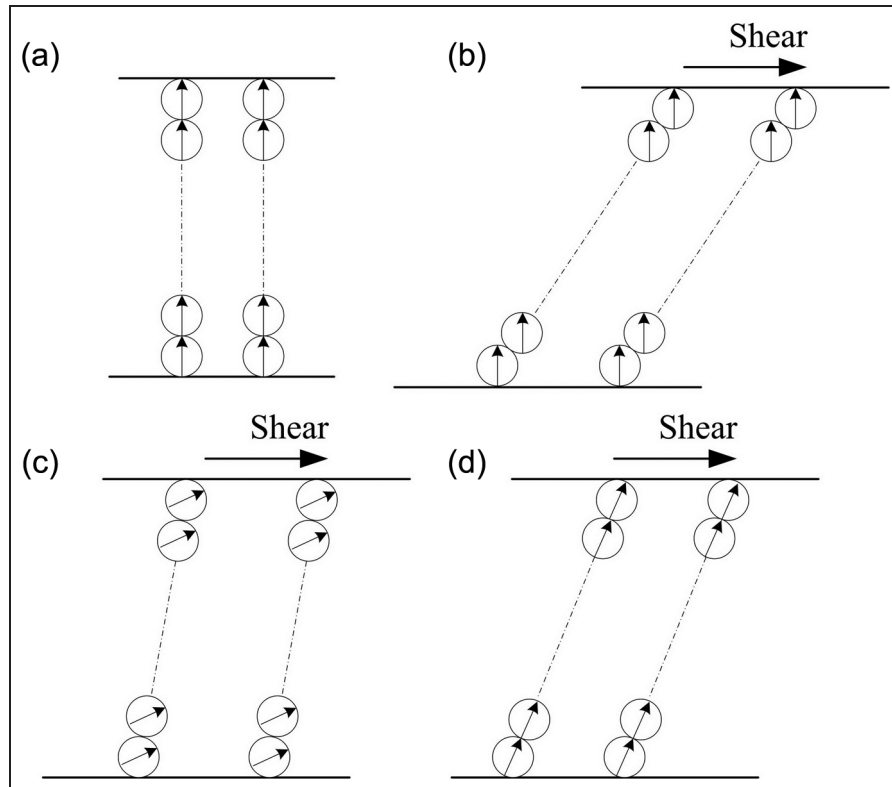


Figure 7. Schematic representation of dielectric relaxation effect on the structure of the ERF: (a) the electric field existing alone, (b) small relaxation time, (c) large relaxation time, and (d) moderate relaxation time.

parallel to the electric field, as shown in Figure 7(a). In this situation, the attraction force between the particles is strongest and the structure of ERFs is the most stable. Then, an external electric field and a shear flow are applied to ERFs. When the relaxation time is too small to ignore the dielectric relaxation effect, the chains are structured with a tilt angle to the direction of the electric dipole moment because of the shear flow (Figure 7(b)). The difference in the direction between the chains and the electric dipole moment makes the chains weaker relative to Figure 7(a). Therefore, the ER effect is indistinctive when the relaxation frequency exceeds 10^5 Hz in Ikazaki's work. When the relaxation time is too large (Figure 7(c)), the particles have a significant dipole moment tilt angle under dynamic shear flow. This results in a tilt angle existing between the electric dipole moment and the chains, and the strength of the chains is not as strong as Figure 7(a). Larger relaxation time leads to a larger angle, which further weakens the structure of ERFs. An overlarge tilt angle will diminish the dipolar force between the rotational particles; even transmit the interparticle force from attractive to repulsive. Therefore, the chains cannot be maintained, the structure of ERFs is destroyed, and the stress decreases signally. Hence, the break shear rate decreases with the increase in the relaxation time when the relaxation time exceeds a certain value. As shown in Figure 7(d), a moderate relaxation time makes the electric dipole

moment parallel to the electric field. Thus, the structure of ERFs is stable and the ERFs achieve a large stress under shear. Therefore, to obtain an obvious ER effect for the ERFs under steady shear flow, the materials should have a proper dielectric property.

Conclusion

The dielectric relaxation effect on the mechanical property and flow behavior of ERFs is investigated by using both computer simulation and experiment investigation. The shear curves of ERFs in the dynamic state were simulated under different relaxation times. The experimental results of the flow curves match the simulation results very well and both indicate the dielectric relaxation effect on ERFs. When the magnitude of the relaxation time is less than 10^{-2} s, the break shear rate changes little at different relaxation times and the structural strength of ERFs is decided by electric and flow field. When the magnitude of the relaxation time is larger than 10^{-2} s, the break shear rate changes obviously and the structural strength is influenced by the relaxation time instead of electric field, leading to the decrease in ER effect. Therefore, the particles of ERFs should have proper dielectric relaxation time to obtain obvious ER effect under steady shear flow. The above work will be useful for understanding the mechanism of ERFs.

Declaration of conflicting interests

The authors declared no potential conflicts of interest with respect to the research, authorship, and/or publication of this article.

Funding

Financial supports from the National Natural Science Foundation of China (Grant No. 11125210) and the National Basic Research Program of China (973 Program, Grant No. 2007CB936800) are gratefully acknowledged.

References

- Cho MS, Choi HJ and Jhon MS (2003) Synthesis and electro-rheological characteristics of polyaniline-coated poly methyl methacrylate microsphere size effect. *Langmuir* 19: 5875–5881.
- Cho MS, Choi HJ and Jhon MS (2005) Shear stress analysis of a semiconducting polymer based electrorheological fluid system. *Polymer* 46: 11484–11488.
- Choi HJ and Jhon MS (2009) Electrorheology of polymers and nanocomposites. *Soft Matter* 5: 1562–1567.
- Choi Y, Sprecher AF and Conrad H (1990) Vibration characteristics of a composite beam containing an electrorheological fluid. *Journal of Intelligent Material Systems and Structures* 1: 91–104.
- Dassanayake UM, Offner SSR and Hu Y (2004) Critical role of flow-modified permittivity in electrorheology: model and computer simulation. *Physical Review E* 69: 021507.
- Davis LC (1992) Polarization forces and conductivity effects in electrorheological fluids. *Journal of Applied Physics* 72: 1334–1340.
- Di K, Zhu YH, Yang XL, et al. (2006) Electrorheological behavior of urea-doped mesoporous TiO₂ suspensions. *Colloids and Surfaces A: Physicochemical and Engineering Aspects* 280: 71–75.
- Gong XL, Yang F, Xuan SH, et al. (2011) Boundary effect in electrorheological fluids. *Physical Review E* 84: 061505.
- Guo HX, Mai ZH and Tian HH (1996) Computer simulation of structures and rheological properties of electrorheological fluids. *Physical Review E* 53: 3823–3831.
- Halsey TC (1992) Electrorheological fluids. *Science* 258: 761–766.
- Hao T (1997) The role of the dielectric loss of dispersed material in the electrorheological effect. *Applied Physics Letters* 70: 1956–1958.
- Hao T and Xu YZ (1996) Correlation of the dispersed particles surface properties with the electrorheological response. *Applied Physics Letters* 69: 2668–2670.
- Hao T, Kawai A and Ikazaki F (1999) Dielectric criteria for the electrorheological effect. *Langmuir* 15: 918–921.
- Ikazaki F, Kawai A, Uchida K, et al. (1998) Mechanisms of electrorheology: the effect of the dielectric property. *Journal of Physics D: Applied Physics* 31: 336–347.
- Jiang WQ, Jiang CX, Gong XL, et al. (2009) Structure and electrorheological properties of nanoporous BaTiO₃ crystalline powders prepared by sol-gel method. *Journal of Sol-Gel Science and Technology* 52: 8–14.
- Jiang WQ, Zhu W, Jiang CX, et al. (2011) The controllable synthesis of nanoporous SrTiO₃ by an ultrasound irradiation approach. *Smart Materials and Structures* 20: 065002.
- Klass DL and Martinek TW (1967) Electroviscous fluids. I. Rheological properties. *Journal of Applied Physics* 38: 67–74.
- Ko YG, Choi US and Chun YJ (2008) Trembling shear behavior of a modified-chitosan dispersed suspension under an electric field and its model study. *Macromolecular Chemistry and Physics* 209: 890–899.
- Melrose JR (1991) Sheared dipolar suspensions. *Physical Review A* 44: R4789–R4792.
- Papadopoulos CA (1998) Brakes and clutches using ER fluids. *Mechatronics* 8: 719–726.
- Parthasarathy M and Klingenberg DJ (1996) Electrorheology: mechanisms and models. *Materials Science & Engineering R: Reports* 17: 57–103.
- Stangroom JE (1983) Electrorheological fluids. *Physics in Technology* 14: 290–296.
- Sun ZH, Wang XX, Soh AK, et al. (2006) On stress calculations in atomistic simulations. *Modelling and Simulation in Materials Science and Engineering* 14: 423–431.
- Tao R and Sun JM (1991) 3-Dimensional structure of induced electrorheological solid. *Physical Review Letters* 67: 398–401.
- Wan JTK, Yu KW and Gu GQ (2000) Dynamic electrorheological effects and interparticle force between a pair of rotating spheres. *Physical Review E* 62: 6846–6850.
- Wang J, Zhao KS and Zhang LP (2013) Dielectric analysis of TiO₂-based electrorheological suspensions. *Rheologica Acta* 52: 115–125.
- Weiss KD, Carlson JD and Coulter JP (1993) Material aspects of electrorheological systems. *Journal of Intelligent Material Systems and Structures* 4: 13–34.
- Wen WJ, Huang XX, Yang SH, et al. (2003) The giant electrorheological effect in suspensions of nanoparticles. *Nature Materials* 2: 727–730.
- Wu JH, Liu FH, Guo JJ, et al. (2012) Preparation and electrorheological characteristics of uniform core/shell structural particles with different polar molecules shells. *Colloids and Surfaces A: Physicochemical and Engineering Aspects* 410: 136–143.
- Yang F, Gong XL, Xuan SH, et al. (2011) Simulation study on the trembling shear behavior of electrorheological fluid. *Physical Review E* 84: 011504.
- Yin JB and Zhao XP (2006) Enhanced electrorheological activity of mesoporous Cr-doped TiO₂ from activated pore wall and high surface area. *Journal of Physical Chemistry B* 110: 12916–12925.